

Outstanding performance of FeNiCoCr-based high entropy alloys: The role of grain orientation and microsegregation

Bao Trung Tran ^a, Hoang Anh Pham ^b, Van Toan Nguyen ^a, Dinh Phuong Doan ^a,
Thi Thanh Thuy Hoang ^c, Nang Xuan Ho ^d, Duy Vinh Nguyen ^d, Tu Le Manh ^{c,*}

^a Institute of Materials Science, Vietnam Academy of Science and Technology, No.18 Hoang Quoc Viet Str., Cau Giay Distr., Hanoi, Viet Nam

^b Faculty of Materials for Energy, Shimane University, 1060 Nishikawatsu-cho, Matsue, Shimane 690-8504, Japan

^c Faculty of Materials Science and Engineering, Phenikaa Institute for Advanced Study (PIAS), Phenikaa University, Hanoi 10000, Viet Nam

^d Faculty of Vehicle Engineering, Phenikaa University, Hanoi, Viet Nam

ARTICLE INFO

Keywords:

High entropy alloys
Super plasticity
Electrocatalyst
Fuel cell
Hydrogen evolution reaction
Corrosion resistance

ABSTRACT

High entropy alloys have presented more interests in energy related applications including catalyst materials. However, the engineering application of these materials is still hindered by lacking information of their mechanical and electrochemical behaviors. Different high-entropy alloys based on FeNiCoCr system (FeNiCoCr, FeNiCoCrCu, and FeNiCoCrMn) were fabricated based on thermodynamic predictions and studied in terms of microstructure and grain orientation in relationship with their mechanical and catalytic properties. The single-phase FCC solid-solutions were obtained in all the fabricated alloys, which have shown excellent ductility during compressive testing. The coarse dendritic microstructure was observed in FeNiCoCr and FeNiCoCrMn alloys, while the finer one was obtained in FeNiCoCrCu, which presented higher value of microhardness. Analyses of EBSD measurements in the studied alloys have shown a strong relationship between the grain orientations and their mechanical behavior. Furthermore, a good corrosion resistance was achieved for the three fabricated alloys, being better the alloy with the addition of Cu element. Among the studied alloys, FeNiCoCrCu has presented excellent electrocatalytic activity and stability toward hydrogen evolution reaction in acidic media. The enhancement in corrosion resistance of FeNiCoCrCu could be associated with presence of {111}//ND component, while its strong catalytic activity is related to the {220}//ND orientation dominated by the material. This outstanding performance of FeNiCoCrCu has demonstrated as a promising candidate to substitute Pt for application as electrocatalyst in acidic media.

1. Introduction

High entropy alloys (HEAs) are classes of new multicomponent materials consisting of five or more principal elements of alloy or have an entropy of mixing higher than 1.5 R [1,2]. HEAs have an increasing interest in many engineering applications because of their outstanding performance and unique properties, namely: high thermal stability, strong mechanical strength, excellent corrosion resistance, fine trade-off effect on performance, and very promising catalyst for hydrogen oxidation reaction (HOR) to enhance the energy conversion efficiency of the hydrogen fuel cell [2–5].

Because the alloys consist of various elements with different percentage representations and foremostly wide range of melting temperatures, there are many techniques used for their preparation. Usually,

HEAs are prepared by arc melting, vacuum induction melting, physical vapour deposition or mechanical alloying (MA), which is accompanied by subsequent compaction via spark plasma sintering (SPS) or hot isostatic pressing (HIP) [6–10].

On the other hand, a vast majority of literatures have reported HEAs as multi-phase alloys, while single phase alloys (solid solutions) with broader applicability have attracted more attention in the practice since important metallurgical variables (i.e., the number, types and concentrations of alloying elements) could be systematically varied and directly correlated with physical-mechanical properties (i.e., elastic constants, stacking-fault energy, diffusion coefficient, strength, and ductility) of the material [11]. However, to achieve the formation of single-phase solid solution alloys from the mixture of five elements in near or equiatomic concentrations is not really simple due to the fact that as per

* Corresponding author.

E-mail address: tu.lemanh@phenikaa-uni.edu.vn (T. Le Manh).

usual, the multicomponent alloys tend to segregate multiple phases and phase transformation during their solidification and heat treatment [12]. Even, in the first single-phase (solid solution) HEAs with faced-center-cubic (FCC) structure reported in the literature, which is known as the quinary CrMnFeCoNi alloy or Cantor alloy [13], it has been found the decomposition into metallic (BCC-Cr) and intermetallic (L10-NiMn and B₂-FeCo) phases at temperature about below 800 °C and heat treatments above 800 °C are required to retain the metastable FCC, solid-solution state at room temperature [11–13]. Previous works have shown more interest in the microstructure examination and the relationship with physical-mechanical properties of HEAs using the combination of different characterization techniques such as scanning electron microscopy (SEM), X-ray diffraction (XRD), transmission electron microscopy (TEM), and electron backscatter diffraction (EBSD) [11–16]. Among these methods, EBSD has been powerful to reveal important information of the material related to microstructure, grain orientations, grain boundary character, and deformation levels, which are fundamental for any (post) treatment proposal and/or modification of processing parameters to improve the respective material's properties [15,16]. Thus, several works have used EBSD to demonstrate the strong influence of the (re)solidification rate on the microstructure and properties of HEA system (Al_xCoCrFeNi, $x = 0 - 1.8$), to analyze microstructural evolution and formation of annealing twins of CoCrFeMnNi after thermomechanical processing, strengthening mechanism of the CoCrFeNiCu HEA via friction stir processing, as well as to investigate microstructures and deformation substructure evolution in FeCoNiCrN alloy [14–19]. Recently, Zhou et al. [20] have found that the addition of anticorrosive elements such as Cr could enhance the corrosion behavior of FeCoCrNi-based HEAs (i.e., CoCrFeMnNi) fabricated by melting, rolling, laser cladding, selective laser melting. This property is also fundamental for the long-term service and stability of the material in any function including electrocatalyst [21]. It is worth mentioning that the application of HAEs as electrocatalyst is a topic of current interest. However, a study dealing with both mechanical and electrochemical behaviors of HAEs is still lacking.

Therefore, this work presents the successful synthesis of single-phased HEA samples, using a simple electric-arc melting method, with not only outstanding mechanical properties (strength, ductility), but also excellent corrosion resistance and electrocatalytic activity in acidic media. The design of the HAEs was performed based on thermodynamic and phase diagram calculations using Thermo-calc software. Mechanical behavior of the studied HAEs was based mainly on Vicker hardness and compression tests. Microstructure and grain orientations determination of the HAEs were studied by SEM, TEM, EBSD measurements. Corrosion behavior and electrocatalytic activity of the HAEs were evaluated using Tafel, cyclic voltammetry, and linear sweep voltammetry techniques.

2. Materials and methods

2.1. Thermodynamic calculations

To predict the solid solution formation of designed alloys, thermodynamic factors are considered including the mixing valence electron concentration (VEC_{mix}), atomic size mismatch (δ_r), enthalpy of mixing (ΔH_{mix}), entropy of mixing (ΔS_{mix}), and parameter Ω , which describes the correlation of enthalpy and entropy of mixing and the mixing melting temperature (T_m). The equations for these thermodynamic factors are as following and generally being used to predict the phase formation in multi-components system [22–24].

$$VEC = \sum c_i VEC_i \quad (1)$$

$$\delta_r = 100\% \left[\sum c_i / (1 - r_i / \bar{r})^2 \right]^{1/2} \quad (2)$$

$$\Delta S_{mix} = -R c_i \ln c_i \quad (3)$$

$$\Delta H_{mix} = \sum 4\omega_{ij} c_i c_j \quad (4)$$

$$\Omega = T_m \Delta S_{mix} / \Delta H_{mix} \quad (5)$$

Here, VEC_i , r_i and T_m are the valence electron concentration, atomic radius and melting temperature of element i ; c_i and c_j correspond to the atomic fractions of element i and j ; \bar{r} is the average atomic radius ($\bar{r} = \sum c_i r_i$); ω_{ij} is the concentration-dependent interaction parameter between elements i and j in a subregular solid solution model, and T_m , the mixing melting temperature is $\sum c_i T_m$.

Equilibrium compositions versus temperature of all phases, which form during solidification of the three alloys, were calculated using Thermo-Calc software using SSOL6 and TCFE9 databases.

2.2. Samples preparation

In this work, the FeNiCoCr, FeNiCoCrMn and FeNiCoCrCu high entropy alloys were fabricated by an electric arc melting equipment. The high purity metals (Fe, Ni, Co, Cr, Mn, and Cu with purity of at least 99.8%) were used as the starting materials. To inhibit the oxidation, the melting chamber was evacuated and refilled with high purity Ar gas (99.99%) for several times, and the Ti-gettered was melted prior to eliminate the residual oxygen in the chamber. The mass of each alloy was calculated to get approximately 20 g ingot. The arc melting was done in a water-cooled copper cavity under high purity Ar atmosphere. To ensure the homogenization of the as-cast alloys, each alloy was remelted five times and flipped for each melt.

2.3. Sample characterizations

Microstructure and crystal structure of the HEAs were studied using SEM, (TEM), and XRD techniques.

The phase component of as-cast alloys was analyzed using an X-ray diffractometer (Bruker D8 Advance Bruker, CuK α radiation, 1.5406 Å). The determination of lattice parameters from XRD data for all the samples was done by the Rietveld refinement method using the Fullprof software.

To observe the microstructure and composition investigation, after grinding with SiC papers, the samples were polished by colloidal diamond suspensions and subsequently etched with H₂O: HNO₃: HCl (the ratio of 6:1:3) solution for few seconds. The microstructure was observed on a field emission scanning electron microscopy (FE-SEM, Hitachi-S4800). The chemical composition and element distribution were analyzed using wavelength dispersive spectroscopy (WDS) in a field-emission electron probe microanalyzer (EPMA, JEOL JXA-8530 F Plus). The elemental mapping and quantitative point measurements were performed using the standard samples of pure elements (99.98%) Fe, Ni, Co, Cr, Mn, and Cu.

For TEM characterization, samples were sectioned in small discs of 3 mm in diameter and 1 mm in thickness, and then ground down to less than 0.1 mm prior to generate a small observation window. TEM images were captured by a high-resolution (HR) TEM (JEM 2100 JEOL, at 200 kV of acceleration voltage) equipped with attachments for selected area electron diffraction (SAED).

The density of the alloys was measured by the Archimedes' principle using a density tester (AND GR 202). The mechanical properties of the specimens were investigated in terms of Vickers hardness (Mitutyo AVK-C0) and compression behavior (AGX-50kNV, Shimadzu) at the room temperature (23 °C). The Vickers hardness was measured under the load of 1 kg (HV1) for a dwelling duration of 15 s. For compression test, the ingot alloys were cut into cylindrical samples with dimensions of 4 mm in diameter and 6 mm in length using a compression rate of $5 \times 10^{-4} \text{ s}^{-1}$ for all samples.

EBSD measurements were performed in the FE-SEM, JEOL JIB-4700 F equipped with an EBSD CMOS detector (Oxford Instrument, Symmetry S2). The EBSD-derived orientation data were analyzed using the TSL OIM Analysis 8.6 software.

Table 1

The calculated parameters: ΔS_{mix} , ΔH_{mix} , VEC_i , and Ω of designed alloys.

Alloys	δ (%)	ΔS_{mix} (kJ K $^{-1}$ mol $^{-1}$)	ΔH_{mix} (kJ mol $^{-1}$)	VEC_i	Ω
FeNiCoCr	0.302	11.526	-7.150	8.25	3.017
FeNiCoCrMn	3.269	13.381	-4.192	8	5.749
FeNiCoCrCu	1.033	13.381	3.248	8.8	7.288

2.4. Electrochemical measurements

Cyclic voltammetry (CV) and linear sweep voltammetry (LSV) were used to evaluate the electrocatalytic activity of the HEAs. The Tafel method was used to study the corrosion behavior of the HEAs. Tafel curves were measured within the potentials ranging from -250 mV to +250 mV respect to the open circuit potential (OCP), with a scan rate of 0.166 mV s $^{-1}$, after when the OCP was stable. All electrochemical tests were performed in 0.5 M H₂SO₄ solution at room temperature using a three-electrode cell. The electrochemical measurements were performed in triplicate to warrant the reproducibility of the experiments. The used acid solution was of analytical grade with pH = 0.3. The studied HAE disks encapsulated by an epoxy resin with an exposed area of 0.077 cm 2 were used as the working electrode (WE), an Ag/AgCl sat. in 3 M KCl was the reference electrode with a Luggin capillary located beneath the WE's surface, and a Pt wire was the counter electrode. The HEAs were mechanically grinded with a series of abrasive silicon carbide grit

papers, then polished with alumina powders. The electrolyte (acidic) solution, the graphite, and Pt electrodes were freshly prepared and cleaned in each experiment to avoid any contamination.

3. Results and discussion

3.1. Thermodynamic calculations

The thermodynamic calculation for designed alloys in this work is shown in Table 1. Parameters such as the atomic radius (r_i), VEC_i , and melting temperature (T_{mi}) of elements were extracted from Ref. [25,26]. ΔH_{mix} was calculated by using a thermodynamic subregular model (Eq. 3) with the parameter ω_{ij} taken from Ref. [27]. Bracq et al. [28] have calculated the enthalpy of mixing for the equiatomic FeNiCoCr and FeNiCoCrMn HEAs, which values were -6.475 and -5.506 kJ/mol, respectively. Those reported values are consistent with the results calculated in the present paper by using a thermodynamic sub-regular model proposed by Takeuchi et al. [27], as the tendency is similar, and the discrepancy is within 1.3 kJ/mol. Therefore, the subregular model can be used for approximation of the enthalpy of mixing in our HEA systems without the need of extensive experimental data or extensive calculations.

The calculation results presented in Table 1 show that all of these designed alloys have the atomic size mismatch (δ_r) less than 6.6%, the ΔH_{mix} in the range of -20–5 kJ mol $^{-1}$ and the parameter Ω larger than

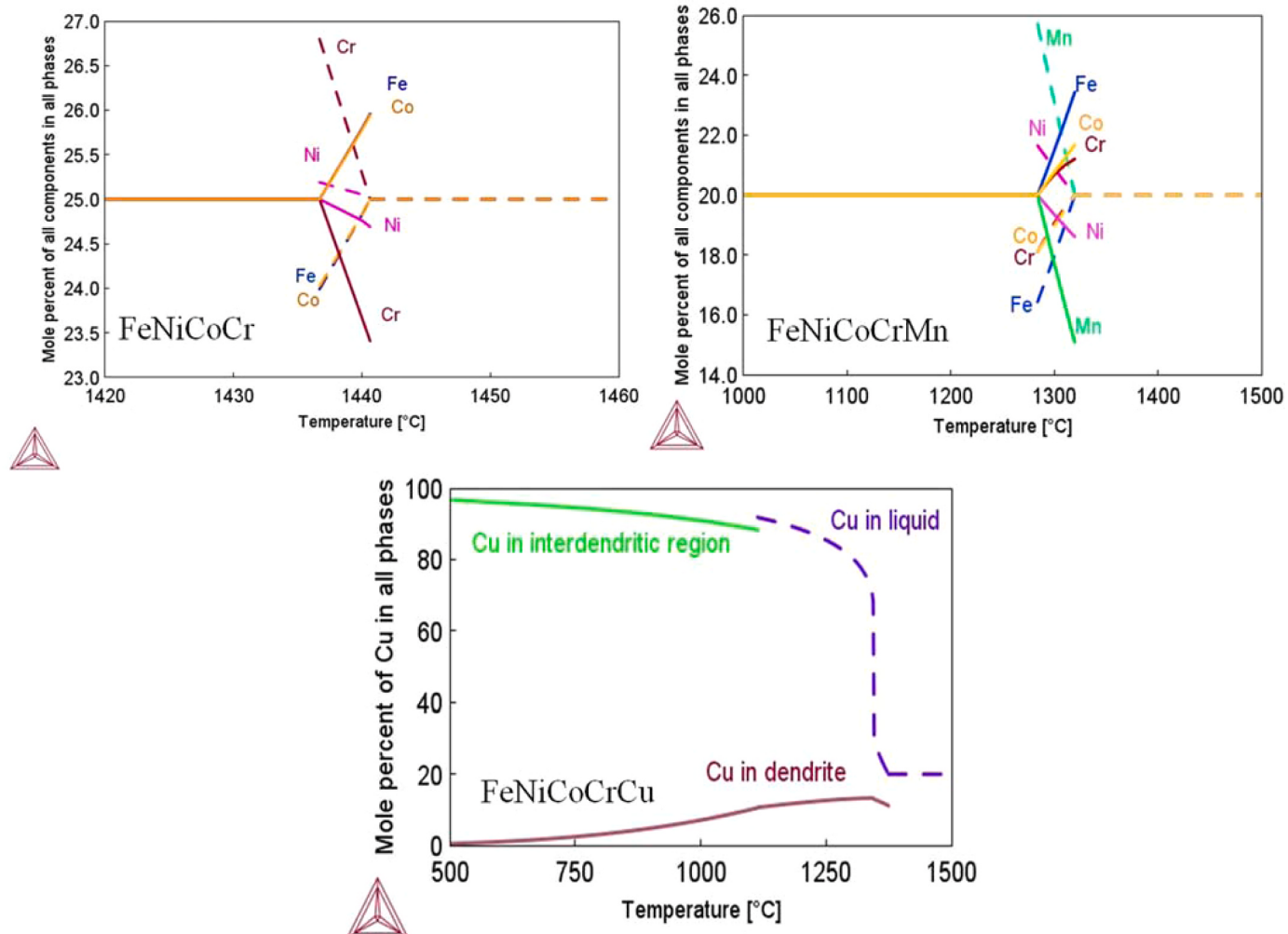


Fig. 1. Composition of liquid and solid phases during equilibrium solidification of the three alloys calculated by Thermo-Calc. Dashed and solid lines represent the mole percent of elements in liquid and solid phases, respectively.

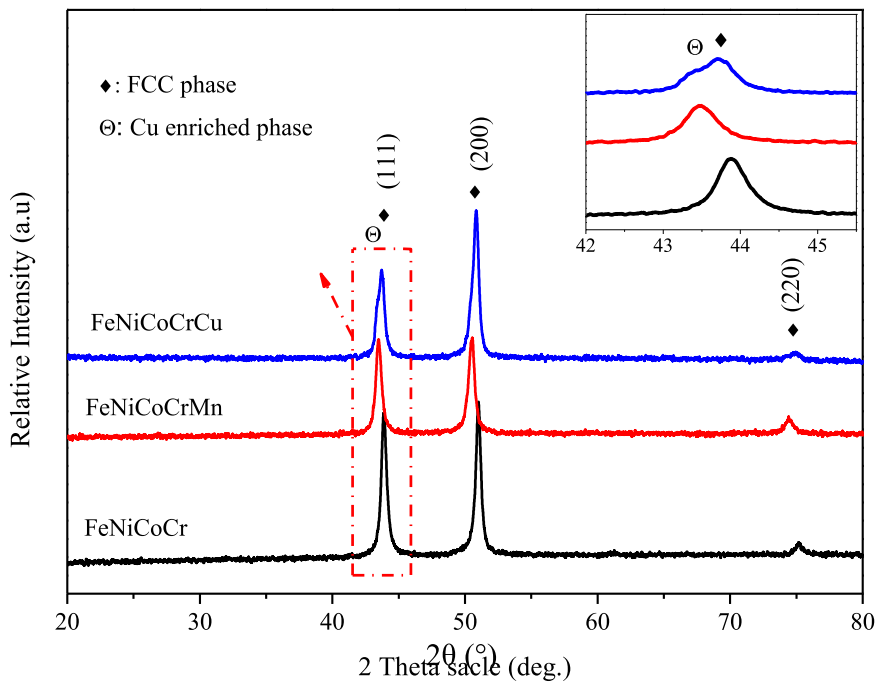


Fig. 2. XRD patterns of as-cast FeNiCoCr, FeNiCoCrMn and FeNiCoCrCu high entropy alloys. The inset depicts an amplified view of diffraction peak related to (111) plane indicated by the red rectangle.

1.1 which prefer the formation of single solid solution of obtained alloys following the summary of Yang *et al.* [23]. Furthermore, the VEC of the alloys are 8.25, 8.0 and 8.8 for FeNiCoCr, FeNiCoCrMn and FeNiCoCrCu respectively indicating the designed alloys are fulfilled for the stabilization of FCC solid solution [24].

To further verify the microstructure formation during casting of the alloys, equilibrium phases and their composition change during the solidification process were theoretically calculated using Thermo-Calc software. Details of equilibrium composition calculated by Thermo-Calc are given in Fig. 1.

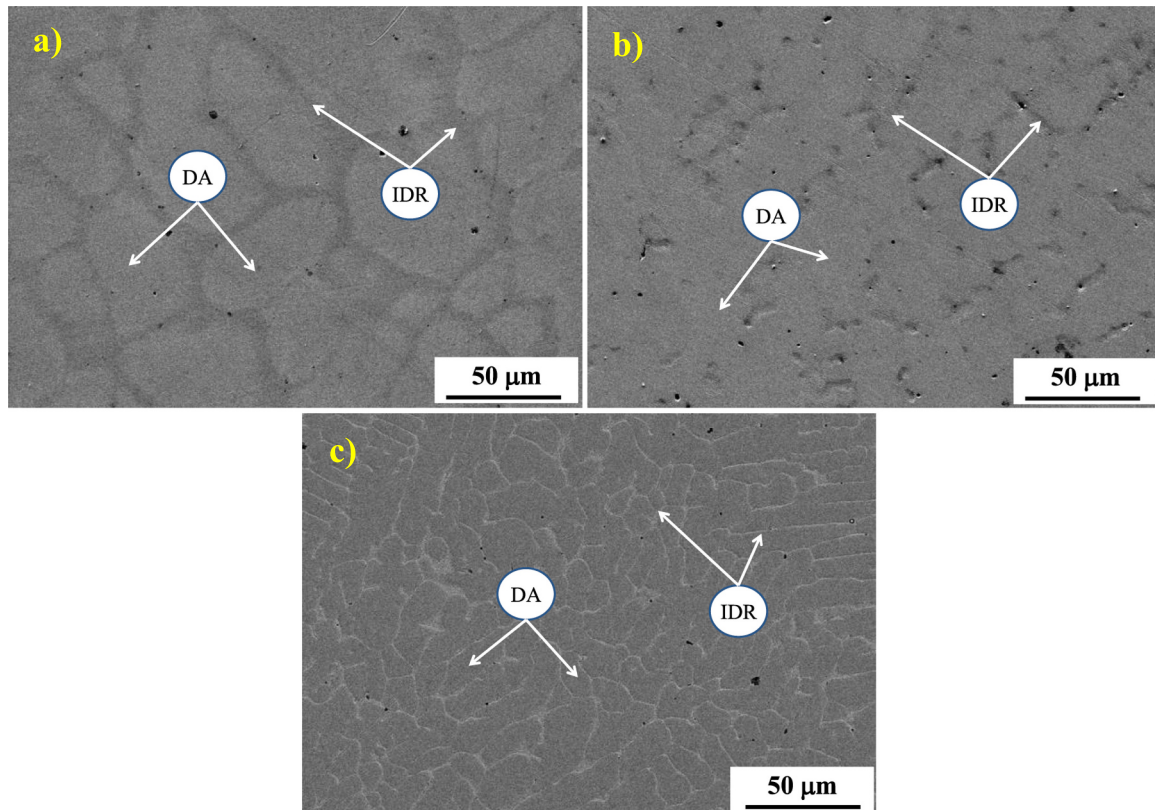


Fig. 3. SEM micrographs of the three HEAs, a) FeNiCoCr, b) FeNiCoCrMn, and c) FeNiCoCrCu.

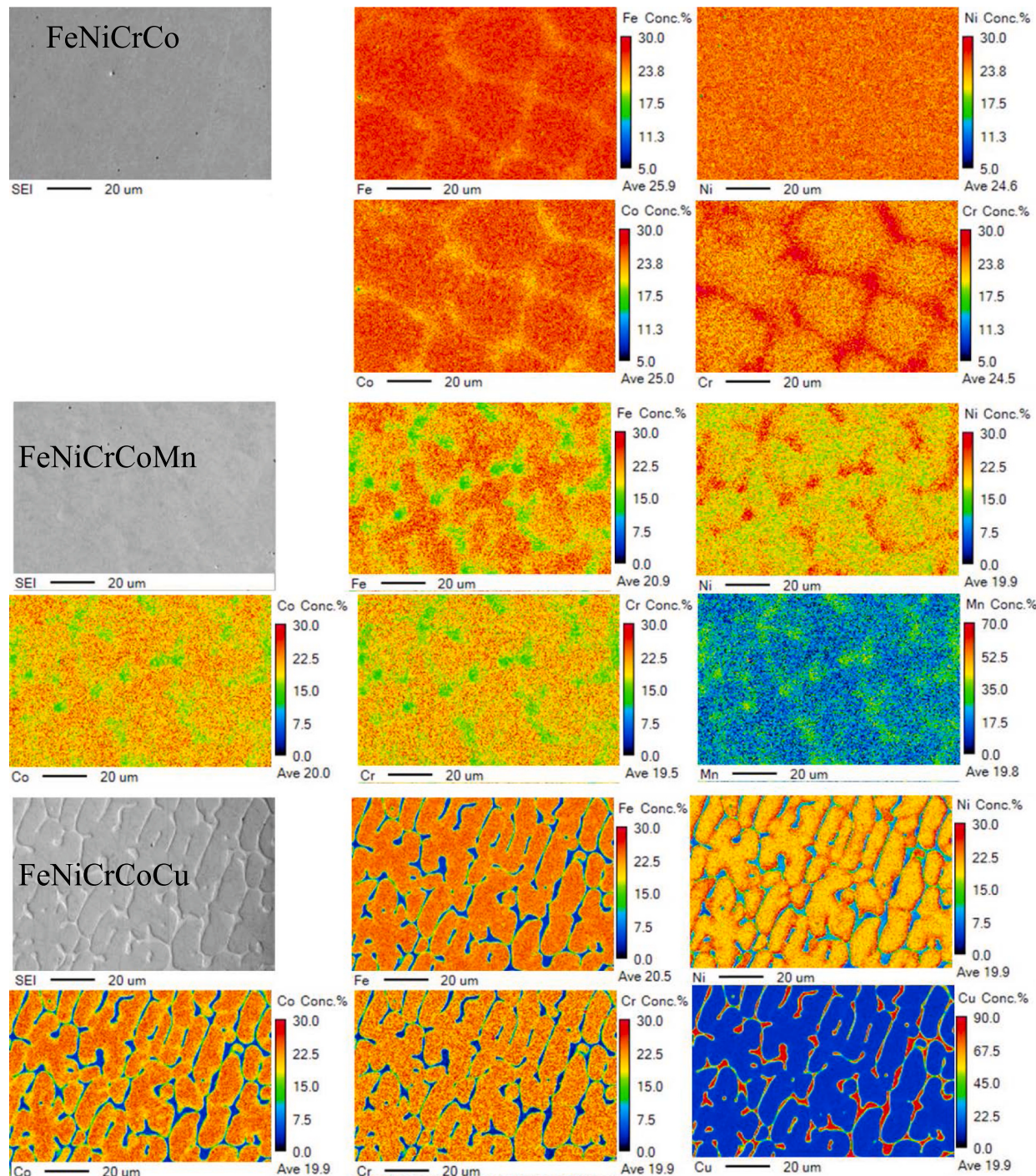


Fig. 4. Quantitative WDS element mapping of the three samples. The color scale bar on the right side of each map, which indicates the atomic percentage of the respective elements is adjusted differently to express the element segregation in the dendritic structure.

The results show the segregation tendency of elements in the equilibrium condition during solidification process. In FeNiCrCo alloy, Cr and Ni diffuse from liquid into the liquid phase, while Fe and Co diffuse into the solid phase. It is expected that a compositional gradient resulted by the elements segregation should promote a dendritic solidification during arc melting of the sample, where a solid FCC phase grows in the dendritic form initially enriched in Fe and Co, with the liquid enriched in Ni and Cr remains in between the dendrite arms - the interdendritic region. The calculation also infers that Cr segregates more readily into the liquid than Ni does, which is consistent with the elemental mapping result presented later in Fig. 4 (WDS map), where Cr is more enriched

than Ni in the interdendritic region (IDR). Similarly, in FeNiCrCoMn alloy, Mn and Ni segregate to the liquid, where Mn is more enriched than Ni. The result is consistent with the WDS elemental mapping (see further in Fig. 4).

However, after the solidification is completed, an equilibrium single FCC phase with equiautomic composition of all elements is expected for both the FeNiCrCo and FeNiCrCoMn alloys (Fig. 1). It suggests that a long homogenization heat treatment should help to remove the micro-segregation of the elements in the as-cast FeNiCrCo and FeNiCrCoMn alloys.

For the FeNiCrCoCu alloy, a different tendency is predicted (Fig. 1).

Table 2

Composition in at% from the DA and IDR zones of the three alloys measured by quantitative WDS.

Sample /Zone analysis		Fe	Ni	Co	Cr	Mn	Cu
FeNiCoCr	DA	26.3 ± 0.1	24.4 ± 0.5	25.9 ± 0.4	23.4 ± 0.8	-	-
	IDR	24.3 ± 0.0	24.9 ± 0.1	23.1 ± 0.3	27.7 ± 0.3	-	-
FeNiCoCrMn	DA	23.4 ± 0.4	18.0 ± 0.5	20.9 ± 0.7	20.5 ± 0.7	17.2 ± 0.7	-
	IDR	13.7 ± 0.5	26.0 ± 0.3	15.2 ± 0.4	14.4 ± 0.8	30.8 ± 1.2	-
FeNiCoCrCu	DA	23.0 ± 0.1	20.1 ± 0.1	24.1 ± 0.1	22.9 ± 0.2	-	9.9 ± 0.1
	IDR	4.1 ± 0.1	9.3 ± 0.1	4.1 ± 0.0	3.3 ± 0.1	-	79.2 ± 0.1

Cu is the only element which strongly segregates into the liquid phase, whereas the other elements segregate into the solid phase. As a result, Fe, Ni, Cr, and Co enriched in solid dendrites with FCC structure, and most of Cu migrates in the liquid which then forms another Cu-enriched phase with FCC structure. After solidification the two FCC phases remain in equilibrium. It suggests that the FeNiCoCrCu alloy is intrinsically dual phase, which will be verified with XRD and WDS analyses (see further in Figs. 3 and 4).

3.2. Structure, chemical composition, and element distribution in as-cast alloys

XRD patterns of as-cast samples are shown in Fig. 2, which clearly indicates that FeNiCoCr and FeNiCoCrMn alloys have only single FCC phase with clear diffraction peaks corresponding to the (111), (200) and (220) crystallographic planes. The FeNiCoCrCu alloy, however, contained two phases in its structure, FCC phase and Cu-enriched FCC phase, which is in agreement with the results of the predicted Thermo-Calc calculations and the previous researches on FeNiCoCrCu HEA alloy [29,30]. For the FCC phases of all as-cast alloys, the calculation of lattice parameters based on Bragg's equation and XRD data (using Rietveld refinement, see Fig. S1) show that the lattice parameters are 3.57, 3.60 and 3.58 Å respective to FeNiCoCr, FeNiCoCrMn and FeNiCoCrCu alloys. Details of these derived parameters using Rietveld refinement can be seen in Table S1 of the Supporting information.

SEM micrographs of the three HEAs in the as-polished and etched are presented in Fig. 3, which clearly depicts the typical dendritic structure of all the alloys. In addition, the coarse dendritic structure was observed for FeNiCoCr and FeNiCoCrMn alloys (Fig. 3a and b), while the finer one is obtained for FeNiCoCrCu (Fig. 3c), which could be due to the strong segregation of Cu to form Cu-enriched phase. For a better observation of element distribution in the dendrite arm (DA) and interdendritic region (IDR) appeared in the structure of each alloy, a more sensible WDS element mapping technique is used, noted that the polished samples without etching were analyzed.

Fig. 4 presents quantitative WDS elemental color mapping images of analyzed areas by electron probe micro-analyzer of all as-cast alloys depicted in Fig. 3. The color scale bar on the right-hand-side of each map, which indicates the atomic percentage of the respective element, is differently adjusted to enhance the contrast from element segregation. The mosaic and the network features on the maps correspond to the dendrite arm (DA) and interdendritic region (IDR), respectively.

The elemental color mapping images clearly show that all the three alloys have a dendritic structure with different degree of element segregation. For FeNiCoCr alloys, the DA is enriched in Fe and Co elements meanwhile the IDR is enriched in Cr. Ni is nearly homogenous in the whole microstructure, but quantitative analysis (Table 2) shows that it is slightly enriched in the IDR. The difference in content of Fe, Cr and Co in DA and IDR is not significant as seen in Table 1. On the other hand,

for FeNiCoCrMn alloy, the DA is rich in Fe, Co, and Cr while the IDR is enriched in Ni and Mn, and the degree of element segregation is larger compared to those for FeNiCoCr alloys, see also in Table 2. The SEM image of FeNiCoCrCu alloy obviously shows the main FCC phase as DA and Cu-enriched fcc phase in the IDR. The average Cu content in FCC phase is approximately 10 at% is much smaller than that of Cu content in Cu-enriched phase, accounted for > 79 at% (Table 2). All the WDS results are consistent well with Thermo-Calc prediction.

In addition to the microstructural analysis by SEM, HRTEM images and SAED patterns were obtained in the studied HEAs as shown in Fig. 5. Fig. 5a, c, e clearly reveal the formation of lattice fringes corresponding to the diffraction planes shown in Fig. 5b, d, f, while electron diffraction rings of SAED patterns (Fig. 5b, d, f) indicate the polycrystalline structure of the HEAs. However, these rings are discontinuous since the number of analyzed grains was small. Interestingly, the analysis of SAED patterns also verifies the single-phase FCC structures of the HEA samples, which are previously determined by XRD measurements. The interplanar spacing (d_{hkl}) values determined by SAED patterns were consistent with XRD measurements (see Table S2) and those reported in literatures [31,32].

3.3. Density and mechanical properties

The FeNiCoCr has a density of approximately (8.18 ± 0.01) g cm⁻³. When Mn was added to obtain the equiatomic FeNiCoCrMn alloy, the density decreased to (7.97 ± 0.01) g cm⁻³ resulted from the lower density of Mn compared to other elements. Meanwhile, the equiatomic FeNiCoCrCu alloy obtained higher density of about (8.26 ± 0.01) g cm⁻³ due to the higher ratio of high-density elements in the alloy composition. Despite the decrease in the density of the designed HEAs, the additions of Mn and Cu in FeNiCoCr system have presented enhancement in mechanical properties as shown in stress-strain curves and microhardness tests of Fig. 6. It reveals that the average Vickers microhardness values of FeNiCoCr, FeNiCoCrMn, and FeNiCoCrCu were determined to be 132.2, 137.2, and 145 HV, respectively (Fig. 6b-d). The higher hardness of FeNiCoCrMn and FeNiCoCrCu alloys compared to FeNiCoCr alloys may be attributed to the solid-solution-like strengthening mechanism originated from the elastic interactions among the local stress fields of solute atoms and dislocations [25,33–35]. In general, the stress-strain curves of as-cast samples in Fig. 6a represent the high ductility of all alloys, which is indicated by the compressive ductility of larger than 50% without fracture. From the recorded data of stress-strain curves, the Young's modulus and 0.2% proof stress ($\sigma_{0.2}$) of as-cast alloys were also derived. The lowest Young's modulus (4.81 GPa) and yield strength (191.8 MPa) values were obtained for the FeNiCoCr alloy. With the addition of Mn or Cu to form equiatomic FeNiCoCrMn and FeNiCoCrCu alloys, both Young's modulus and 0.2% proof stress increased and reached the highest values of 9.4 GPa, and 298.2 MPa, respectively, for FeNiCoCrCu alloy.

The enhancement of Young's modulus and 0.2% proof stress by the addition of Mn and Cu may be resulted from the solid-solution-like strengthening mechanism as mentioned above. Furthermore, the appearance of Cu led to the segregation of Cu - enriched phase could promote the strengthening factor and result in the highest value of Young's modulus and 0.2% proof stress of FeNiCoCrCu alloy. Table 3 summarized the 0.2% proof stress, compressive ductility, and hardness of HEAs in this work and previous reports produced by vacuum arc melting route, which shows the high compressive ductility larger than 50% without fracture for all three alloys with an agreement with other reports [36–43]. A similar trend has been observed that the strength of the alloys, which increase in the order of FeNiCoCr, FeNiCoCrMn and FeNiCoCrCu. The values of 0.2% proof stress, compressive ductility, and hardness of HEAs in this work are comparable with those reported in the literature according to the comparison shown in Table 3.

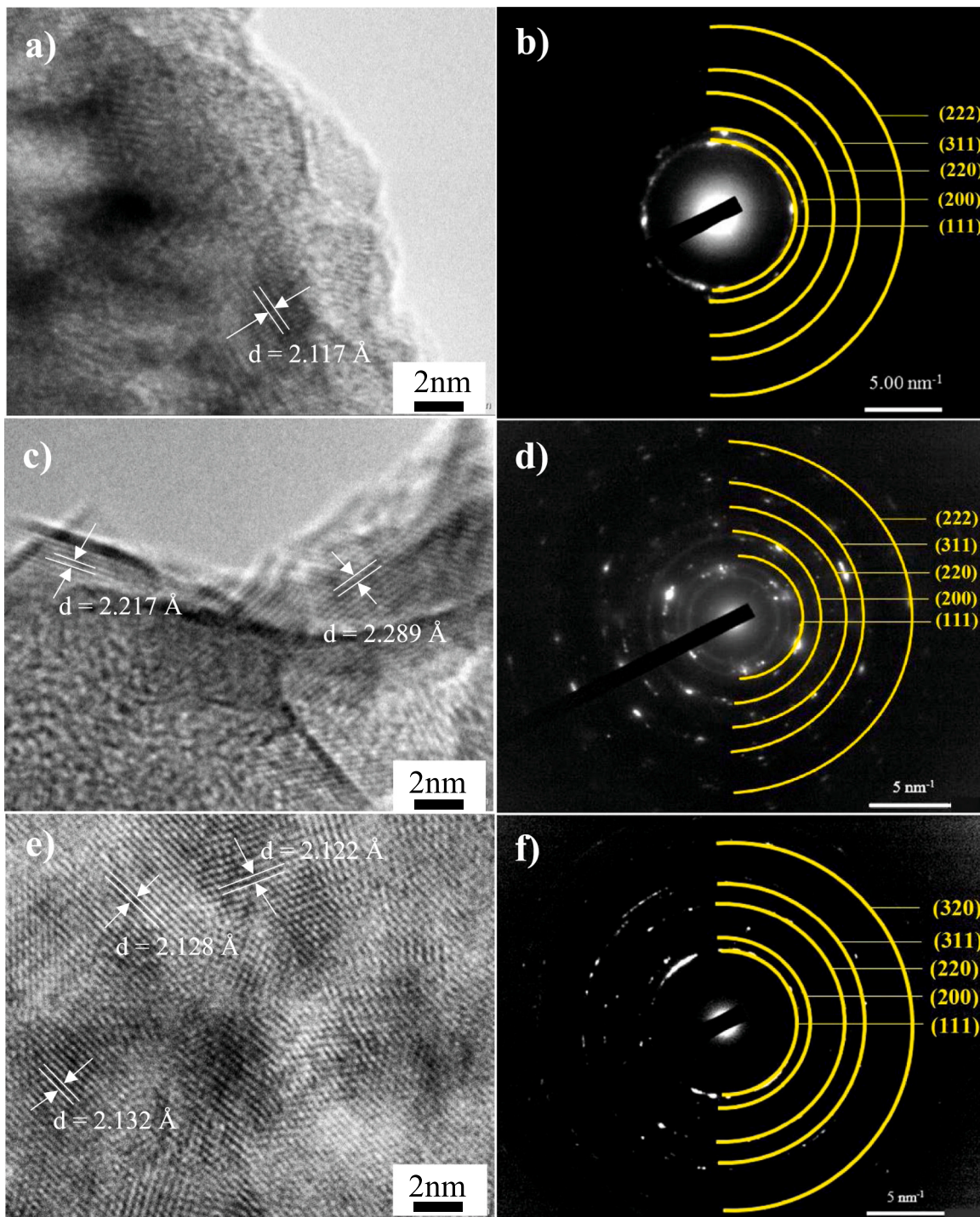


Fig. 5. HRTEM images and SAED patterns of as-cast HEAs: a, b) FeNiCoCr, c, d) FeNiCoCrMn, e, f) FeNiCoCrCu.

3.4. Analysis of crystallographic (grain) orientations

EBSD maps of HEAs in Fig. 7 have shown different behavior in grain's morphologies and orientations. Thus, in general, large grains with average sizes of 259.3 μm , 88.5 μm , and 66.8 μm are observed for FeNiCoCr, FeNiCoCrMn, and FeNiCoCrCu, respectively. The reduction in grain size could contribute to the enhancement in mechanical strength (hardness, Young modulus) according to Hall-Petch equation [44]. Moreover, Fig. 7d exhibits a high fraction of high-angle grain boundaries (HAGBs), which were determined to be about 63%, 73%, and 75%, for FeNiCoCr, FeNiCoCrMn, and FeNiCoCrCu, respectively.

The increase in fractions of HAGBs from FeNiCoCr to FeNiCoCrCu could be explained due to the reduction in grain sizes previously observed in these materials. Meanwhile, Li et al. [45] suggest that when these number fractions of HAGBs are within the range of 60–80%, the HEAs processing should be associated with a continuous dynamic recrystallization.

On the other hand, the analysis of grains orientation derived from EBSD maps reveals that both FeNiCoCr and FeNiCoCrMn alloys exhibit orientations close to {200} // ND (denoted by red color in the standard triangle) (see Fig. 7a, b). Individually, in the case of FeNiCoCrMn the grain orientations along {220} // ND are notable, while {111} // ND

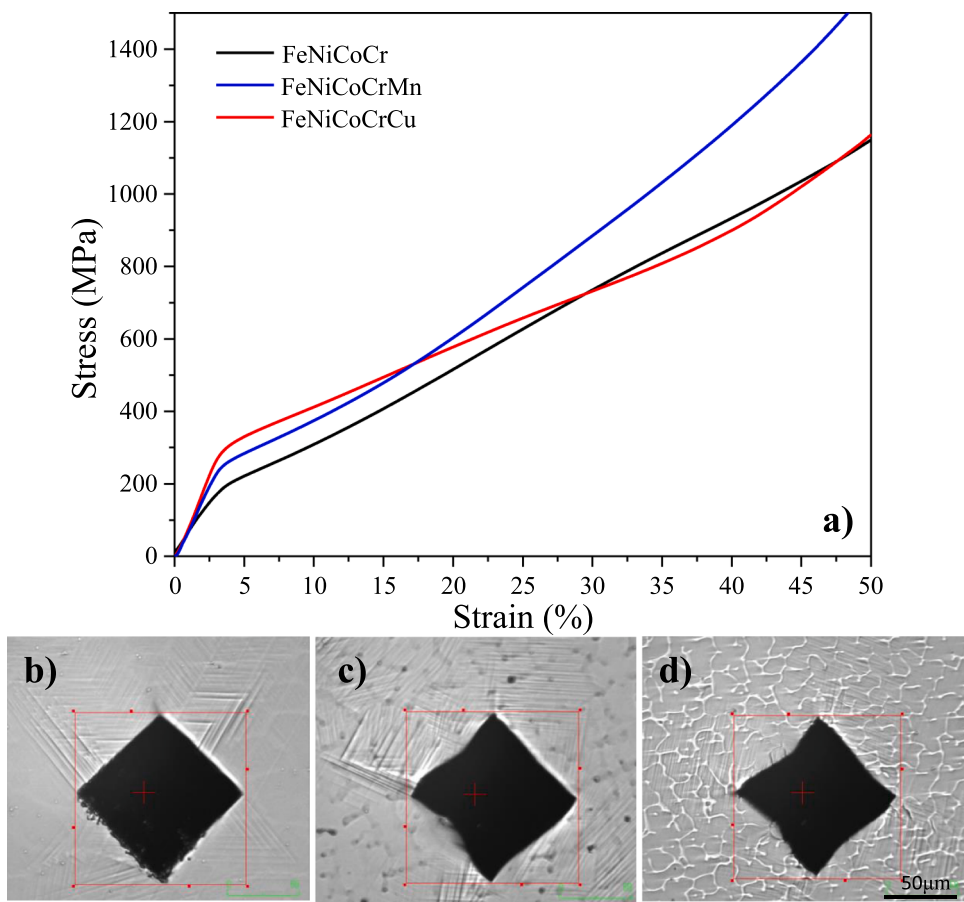


Fig. 6. a) Compression stress-strain curves of the as-cast FeNiCoCr, FeNiCoCrMn and FeNiCoCrCu HAE alloys; Representative microhardness indentation marks of b) FeNiCoCr, 132 HV, c) FeNiCoCrMn, 137 HV, and d) FeNiCoCrCu alloys, 148 HV.

Table 3

Comparison of the 0.2% proof stress, compressive ductility, and hardness of different HEAs.

Alloys	$\sigma_{0.2}$ (MPa)	ε_f (%)	Hardness (HV)	References
FeNiCoCr	190	> 75	160 ± 4	[36]
	136	75	-	[37]
	145	> 50	~150	[38]
	191.8	> 50	132.2 ± 4.1	This work
FeNiCoCrMn	202	> 50	-	[39]
	230	> 50	144 ± 3	[40]
	216	> 50	-	[41]
	207.9	> 50	137.2 ± 2.9	This work
FeNiCoCrCu	230	50.2	-	[42]
	338	> 50	-	[43]
	298.2	> 50	145 ± 2	This work

component is dominant in FeNiCoCr alloy. On the other hand, only FeNiCoCrCu alloy clearly exhibits both {222}//ND and {220}//ND orientations (Fig. 7c). It is important to note the presence of these components in the HEAs help to enhance the ductility and plasticity of the material on the plane indicated in Fig. 7. Thus, in FCC metals, the slip and twinning systems, occurring along close packed plane, are {111} < 110 > and {111} < 112 >, respectively [46]. These systems are observed to be active in all the studied HEAs, resulting in a better resistance against deformation due to the stress relaxation mechanism through dislocation motion [47], and consequently a good ductility of the HEAs (see Table 2).

3.5. Corrosion behavior

Fig. 8 shows the Tafel curves of HEAs in 0.5 M H₂SO₄ solution. Corrosion parameters such as corrosion potential, E_{corr} , and corrosion current density, j_{corr} , derived from Tafel curves are obtained in Table 4. In general, all the obtained HEAs have presented better corrosion resistance than a similar alloy produced by the 3D printing using selected laser melting (SLM) method. Thus, j_{corr} of the SLM HAE alloy was of 58.9 $\mu\text{A cm}^{-2}$ [20], much higher than those reported in the present work.

From Table 2, it can be observed that from thermodynamic point of view, FeNiCoCrMn tends to corrode more easily compared to the other two HEAs because of the more negative E_{corr} . The same tendency remains from kinetic point of view since the larger j_{corr} of the three HEAs corresponds to FeNiCoCrMn. Moreover, FeNiCoCrCu alloy (with smaller j_{corr} value, 2.70 $\mu\text{A cm}^{-2}$) slightly improves the corrosion resistance of FeNiCoCr ($j_{corr} = 2.80 \mu\text{A cm}^{-2}$), while it decreases significantly in the case of FeNiCoCrMn ($j_{corr} = 7.94 \mu\text{A cm}^{-2}$). This enhancement in corrosion resistance of FeNiCoCrCu could be due to the two-passivation processes observed in the anodic branch of Fig. 8.

Moreover, it is generally believed that the surface energy, γ , of different crystallographic planes in FCC crystal such as HEAs follows the trend $\gamma(111) < \gamma(100) < \gamma(110)$ [48]. Therefore, according to the orientation analyses, the improvement in corrosion resistance of FeNiCoCrCu and FeNiCoCr compared to FeNiCoCrMn can be associated with the presence of {222}//ND and {200}//ND grain orientations with lower surface energies (more compact planes) than the {220}//ND component of FeNiCoCrMn. Effectively, the intensity of (220) peak of FeNiCoCrCu, which has the better corrosion resistance, is slightly smaller than the rest of samples.

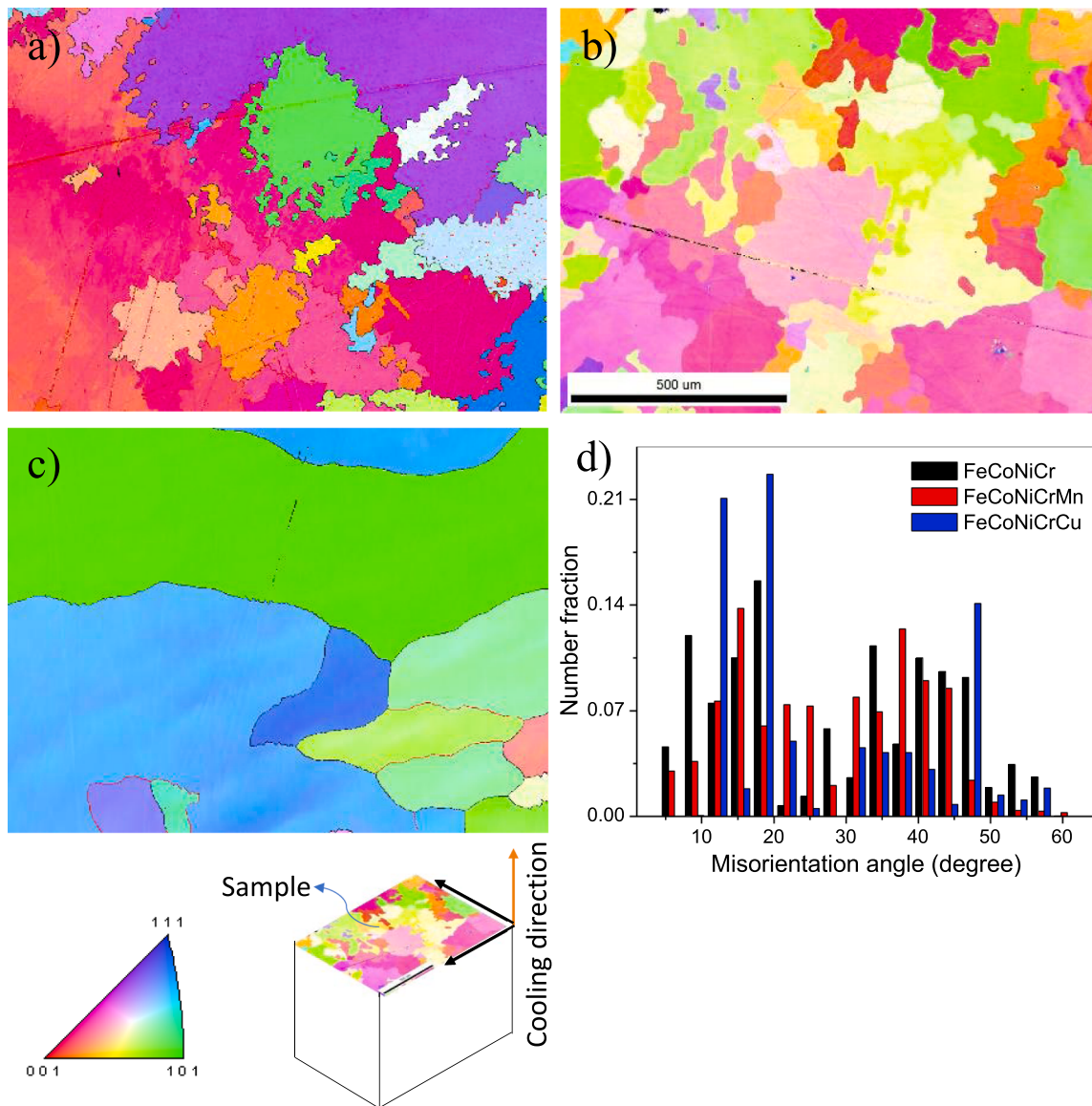
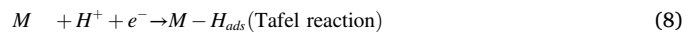
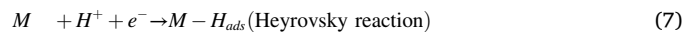
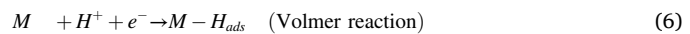


Fig. 7. Orientation maps of HEAs alloys, a) FeNiCoCr, b) FeNiCoCrMn, c) FeNiCoCrCu, and d) Misorientation angle distribution of Fig. 6a-c.

3.6. Catalytic behavior

Fig. 9 shows a better performance of FeNiCoCr toward hydrogen evolution reaction (HER) reaction compared to the other HEAs. At a current density of $j = -7 \text{ mA cm}^{-2}$, the onset potentials toward HER determined for these materials are: $E(\text{Pt}) = -0.27 \text{ V}$, $E(\text{FeNiCoCrCu}) = -0.49 \text{ V}$, $E(\text{FeNiNoCr}) = -0.54 \text{ V}$, and $E(\text{FeNiNoCrMn}) = -0.61 \text{ V}$. It can be clearly seen that based on the previous potentials Pt has shown to be the most active material for HER, then follows the HEAs with the following sequence: Pt > FeNiCoCrCu > FeNiNoCr > FeNiNoCrMn. It is important to note that FeNiNoCrCu has presented better catalytic activity than FeNiNoCr, which is reported in [49] to have a closer HER activity to Pt than its individual components. This enhancement could be attributed to partial oxidation of Cr, Fe, and Co on the surface, providing weak binding energy or weak adsorption to atomic hydrogen (H) [49] and the addition of copper element in the alloy, as well. In addition, Fig. 9b clearly shows that the Tafel slopes of the HEAs in acidic solution follow the order: FeNiNoCr (58 mV dec^{-1}) > FeNiNoCrMn (49 mV dec^{-1}) > FeNiCoCrCu (39 mV dec^{-1}) > bulk Pt (19 mV dec^{-1}). Considering low Tafel slope values means a strong catalytic activity of the material toward HER [49,50], one can observe that FeNiCoCrCu

with a small slope value, closer to Pt, becomes the better one among the studied HEAs. It is widely accepted that in acidic media HER could involve the following reaction steps given by Eqs. (6–8) [51–53].



Where: M and $M - H_{ads}$ refer to a vacant surface site of the electrocatalyst and the absorbed hydrogen atoms, respectively. According to several literatures, the low Tafel slope values of the studied HEAs obtained in $0.5 \text{ M H}_2\text{SO}_4$ solution suggest that HER could be occurred via the Volmer–Heyrovsky mechanism [51–53].

Like corrosion behavior (see Section 3.4), the surface energy of the crystallographic plane plays an important role in the electrocatalytic activity of the HEAs. It is known that the presence of high-surface energy of crystal facets leads to greater reactivity and thereby better catalytic efficiency [50]. From EBSD orientation maps, the better performance of FeNiCoCrCu could be related to the presence of $\{220\}/\text{ND}$ orientations, while the lower efficiency of the rest of samples should be due to the

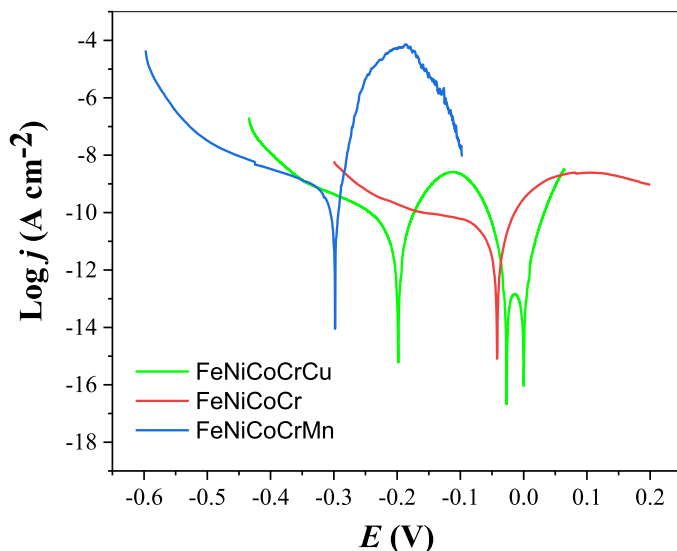


Fig. 8. Tafel curves of the studied HEA alloys in 0.5 M H_2SO_4 solution.

Table 4
Electrochemical parameters obtained from the potentiodynamic polarisation tests.

Samples	β_a (mV)	β_c (mV)	j_{corr} (μAcm^{-2})	E_{corr} (mV)
FeNiCoCrCu	36	103	2.70	-198
FeNiCoCr	52	236	2.80	-42
FeNiCoCrMn	12	139	7.94	-298

dominance of {200}//ND components.

On the other hand, the reduction in the catalytic performance of the FeNiNoCrMn compared to the based alloy, FeNiNoCr, could be due to the incorporation of manganese in the HAE. Thus, it is well-known that Mn is good for wear and abrasion resistance properties, but it is considered to have a negative effect on the corrosion resistance of stainless steel as it tends to weaken the passive film, forming pitting in the steel surface [54]. As can be observed in WDS element mapping of Fig. 2, manganese is distributed with high concentration in the grain boundary, which is also detrimental for pitting resistance.

The stability of HEAs in acidic media was tested by CV at 20 mVs^{-1} in 0.5 M H_2SO_4 solution as shown in Fig. 10. It reveals a decrease in the current density at 100 cycles, after that all the CV remains stable. In

general, excellent stability was observed for FeNiCoCrCu and FeNiCoCr alloys, while FeNiCoCrMn is not stable in acidic media. The decrease in current density could be due to the oxidation and dissolution of metallic element of the HAE during the test, which is evident in the case of FeNiCoCrMn (the solution slightly turns to yellow color after the test). The CV shape and stability behavior of FeNiCoCr in this work agrees with that observed in Ref. [49]. Also from this work, this good stability could be due to the presence of Cr in the alloy since the HAE dissolution should start first from the corrosion resistant element such as Cr, which produces a thin shell of Cr_2O_3 that helps to protect material from penetration of corrosive environment. The good catalytic activity, stability, toward HER and good corrosion resistance of FeNiCoCrCu in acidic media presented in this work suggests its potential application as electrocatalyst for hydrogen fuel cells.

4. Conclusions

In this work, both thermodynamic calculations and experiments were performed for the design of different HEAs (FeNiCoCr, FeNiCoCrMn and FeNiCoCrCu). The synthesis of HEAs was successfully achieved by electric arc melting process. Thermodynamic calculations have shown that solid solution could be formed for all designed alloys. The Thermo-calc calculation predicts the formation of single FCC phase for FeNiCoCr and FeNiCoCrMn alloys with dendrite structure, meanwhile the FeNiCoCrCu have 2 phases: FCC and Cu-enriched FCC phase by the stronger segregation of Cu element. The experimental results showed an agreement with the thermodynamic calculation about the formation of single FCC phase for FeNiCoCr and FeNiCoCrMn alloys, and two-phase structure for FeNiCoCrCu alloy, evidenced with the XRD patterns, SEM, TEM images as well as the EPMA analyses. The obtained HEAs were characterized by the formation of single phase with excellent mechanical properties. The compression tests indicated the good plastic deformation of all designed alloys revealing by the compressive ductility of larger than 50% without fracture, which agrees with previous reports on these alloys. Besides, the addition of Mn or Cu into FeNiCoCr led to an improvement of Young's modulus, 0.2% proof stress and Vickers microhardness of FeNiCoCrMn and FeNiCoCrCu alloys, which could be attributed to the solid-solution-like strengthening mechanism. The excellent ductility during compressive testing of these alloys could be caused by formation of single-phase faced-centered-cubic solid solution structure and the preferred growth along {200} and {220} crystallographic planes for FeNiCoCr, FeNiCoCrMn and FeNiCoCrCu, respectively, and their high fraction of high-angle grain boundaries. According to the electrochemical testing results, the three HEAs have presented good corrosion resistance in acidic solution (0.5 M H_2SO_4), with the

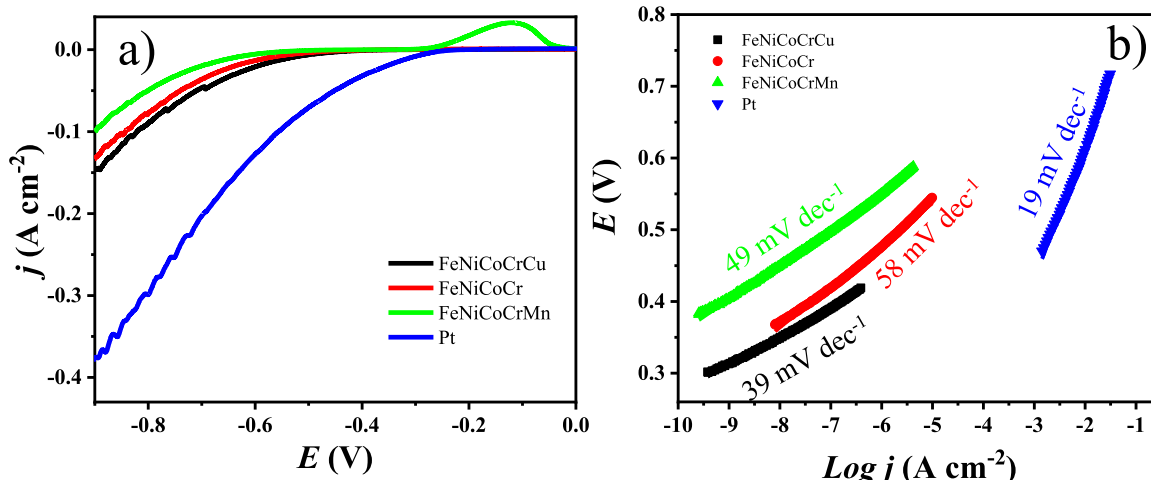


Fig. 9. a) LSV curves and b) Tafel plots of HEAs in acidic media.

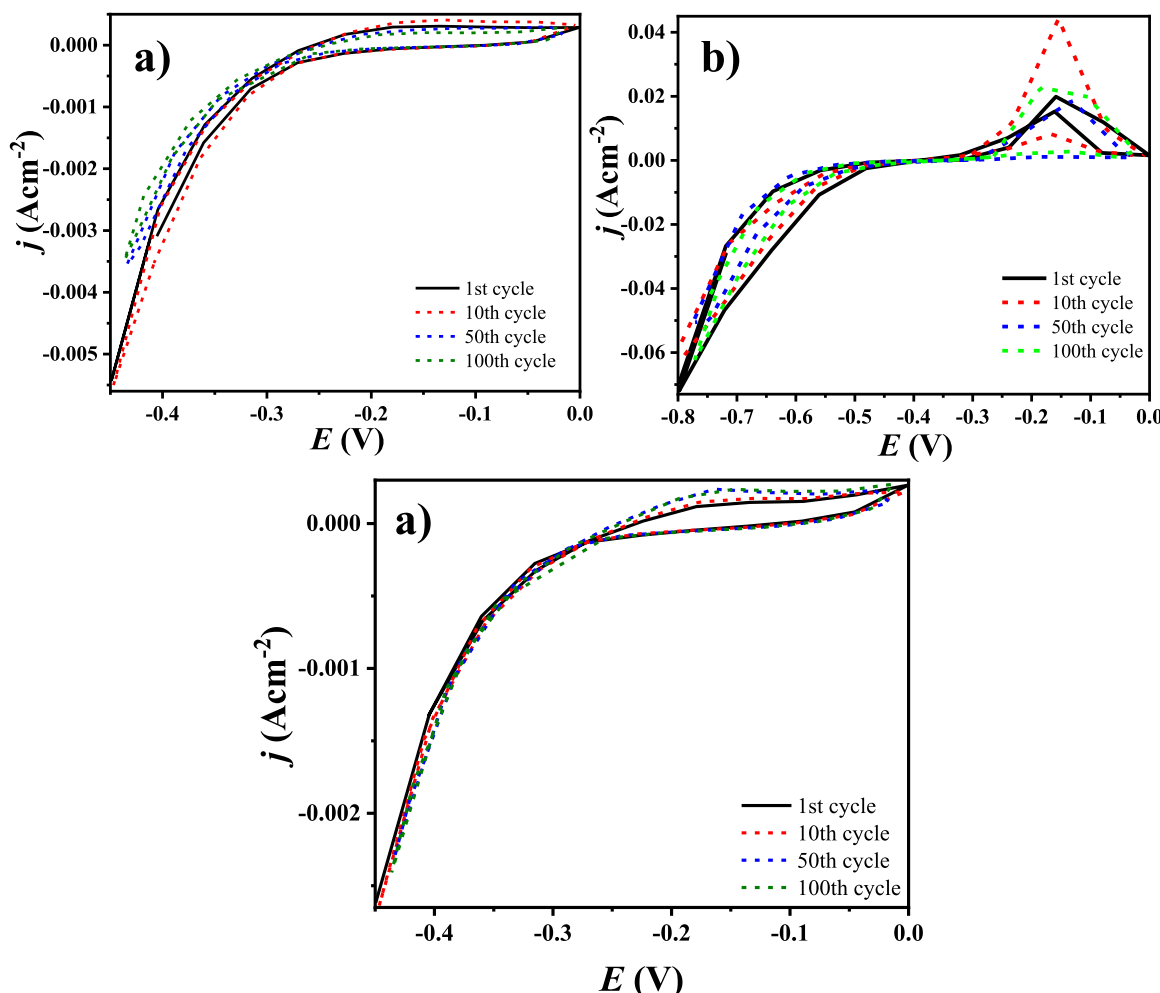


Fig. 10. Stability test of HEAs in acidic media, a) FeNiCoCrCu, b) FeNiCoCrMn, c) FeNiCoCr.

following order: FeNiCoCrCu > FeNiCoCr > FeNiCoCrMn. Moreover, strong catalytic activity for HER was observed in the three HEAs where FeNiCoCrCu was the material that presented closer behavior with Pt. This material also exhibited good stability in acidic media, which could be promising for the application as electrocatalyst in fuel cells. The enhancement in corrosion resistance of FeNiCoCrCu could be associated with the presence of the {111}//ND component, while its strong catalytic activity is related to the {220}//ND orientation dominated by the material.

CRediT authorship contribution statement

Tran Bao Trung: Conceptualization, Format analysis, Methodology, Resources, Writing – original draft, Writing – review & editing. **Hoang Anh Pham:** Funding acquisition, Investigation, Writing – review & editing. **Nguyen Van Toan:** Methodology, Data curation. **Doan Dinh Phuong:** Format analysis, Investigation. **Hoang Thi Thanh Thuy:** Data curation, Format analysis, Investigation. **Ho Xuan Nang:** Project administration, Format analysis, Writing – review & editing. **Nguyen Duy Vinh:** Data curation, Format analysis, Resources. **Tu Le Manh:** Conceptualization, Investigation, Format analysis, Supervision, Project administration, Writing – original draft, Writing – review & editing.

Declaration of Competing Interest

The authors declare that they have no known competing financial interests or personal relationships that could have appeared to influence

the work reported in this paper.

Data Availability

Data will be made available on request.

Acknowledgments

The authors would like to thank the support from Phenikaa Innovation Foundation under the grant No. ĐMST-2022.01.

Appendix A. Supporting information

Supplementary data associated with this article can be found in the online version at doi:10.1016/j.jallcom.2023.172860.

References

- [1] E.P. George, D. Raabe, R.O. Ritchie, High-entropy alloys, *Nat. Rev. Mater.* 4 (2019) 515–534.
- [2] T.R. Paul, I.V. Belova, G.E. Murch, Analysis of diffusion in high entropy alloys, *Mater. Chem. Phys.* 210 (2018) 301–308.
- [3] C. Wagner, G. Laplanche, Effects of stacking fault energy and temperature on grain boundary strengthening, intrinsic lattice strength and deformation mechanisms in CrMnFeCoNi high-entropy alloys with different Cr/Ni ratios, *Acta Mater.* 244 (2023), 118541.
- [4] Y. Xin, S. Li, Y. Qian, W. Zhu, High-entropy alloys as a platform for catalysis: progress, challenges, and opportunities, *ACS Catal.* 10 (2020) 11280–11306.

- [5] C. Zhan, Y. Xu, L. Bu, H. Zhu, Y. Feng, T. Yang, Y. Zhang, Z. Yang, B. Huang, Q. Shao, X. Huang, Subnanometer high-entropy alloy nanowires enable remarkable hydrogen oxidation catalysis, *Nat. Commun.* 12 (2021) 6261.
- [6] Y. Zhang, T.T. Zuo, Z. Tang, M.C. Gao, K.A. Dahmen, P.K. Liaw, Z.P. Lu, Microstructures and properties of high-entropy alloys, *Prog. Mater. Sci.* 61 (2014) 1–93.
- [7] M.C. Gao, J.W. Yeh, P.K. Liaw, Yong Zhang, Fabrication Routes. High-Entropy Alloys: Fundamentals and Applications, Springer International Publishing, 2016, pp. 151–179.
- [8] X. Yang, S. Chen, J.D. Cotton, Y. Zhang, Phase stability of low-density, multiprincipal component alloys containing aluminum, magnesium, and lithium, *JOM* 66 (2014) 2009–2020.
- [9] M. Vaidya, G.M. Muralikrishna, B.S. Murty, High-entropy alloys by mechanical alloying: a review, *J. Mater. Res.* 34 (2019) 664–686.
- [10] A. Strakosova, P. Kratochvil, J. Riedl, F. Průša, Phase and mechanical properties response of the mechanically alloyed CoCrFeNiAlX high entropy alloys, *Manuf. Technol.* 22 (2022) 471–476.
- [11] C. Chu, W. Chen, Z. Chen, Z. Jiang, Microstructure and mechanical behavior of FeNiCoCr and FeNiCoCrMn high-entropy alloys fabricated by powder metallurgy, *Acta Metall. Sin.* 34 (2021) 445–454.
- [12] C.L. Tracy, S. Park, D.R. Rittman, S.J. Zinkle, H. Bei, M. Lang, R.C. Ewing, W. L. Mao, High pressure synthesis of a hexagonal close-packed phase of the high-entropy alloy CrMnFeCoNi, *Nat. Commun.* 8 (2017) 15634.
- [13] B. Cantor, I.T.H. Chang, P. Knight, A.J.B. Vincent, Microstructural development in equiatomic multicomponent alloys, *Mater. Sci. Eng. A* 375–377 (2004) 213–218.
- [14] F. Otto, N.L. Hanold, E.P. George, Microstructural evolution after thermomechanical processing in an equiatomic, single-phase CoCrFeMnNi high-entropy alloy with special focus on twin boundaries, *Intermetallics* 54 (2014) 39–48.
- [15] P.P. Bhattacharjee, G.D. Sathiaraj, M. Zaid, J.R. Gatti, C. Lee, C.W. Tsai, J.W. Yeh, Microstructure and texture evolution during annealing of equiatomic CoCrFeMnNi high-entropy alloy, *J. Alloy. Compd.* 587 (2014) 544–552.
- [16] Z. Li, K.G. Pradeep, Y. Deng, D. Raabe, C.C. Tasan, Metastable high-entropy dual-phase alloys overcome the strength–ductility trade-off, *Nature* 534 (2016) 227–230.
- [17] V. Ocelik, N. Janssen, S.N. Smith, J.T.H.M. De Hosson, Additive manufacturing of high-entropy alloys by laser processing, *JOM* 68 (7) (2016) 1810–1818, <https://doi.org/10.1007/s11837-016-1888-z>.
- [18] C. Chu, W. Chen, Z. Chen, Z. Jiang, H. Wang, Z. Fu, Microstructure and mechanical behavior of FeNiCoCr and FeNiCoCrMn high-entropy alloys fabricated by powder metallurgy, *Acta Metall. Sin.* 34 (2021) 445–454.
- [19] Z. Wang, J. Gu, D. An, Y. Liu, M. Song, Characterization of the microstructure and deformation substructure evolution in a hierarchical high-entropy alloy by correlative EBSD and ECCI, *Intermetallics* 121 (2020), 106788.
- [20] R. Zhou, W. Chen, W. Li, T.H. Chou, Y.H. Chen, X. Liang, J. Luan, Y. Zhu, J. C. Huang, Y. Liu, et al., 3D printed N-doped CoCrFeNi high entropy alloy with more than doubled corrosion resistance in dilute sulphuric acid, *NPJ Mater. Degrad.* 7 (2023) 8.
- [21] H. Li, Y. Han, H. Zhao, W. Qi, D. Zhang, Y. Yu, W. Cai, S. Li, J. Lai, B. Huang, L. Wang, Fast site-to-site electron transfer of high-entropy alloy nanocatalyst driving redox electrocatalysis, *Nat. Commun.* 11 (2020) 5437.
- [22] A. Amiri, R. Shahbazian-Yassar, Recent progress of high-entropy materials for energy storage and conversion, *J. Mater. Chem. A* 9 (2021) 782–823.
- [23] X. Yang, Y. Zhang, Prediction of high-entropy stabilized solid-solution in multi-component alloys, *Mater. Chem. Phys.* 132 (2012) 233–238.
- [24] S. Guo, C.T. Liu, Phase stability in high entropy alloys: Formation of solid-solution phase or amorphous phase, *Prog. Nat. Sci.: Mater.* 21 (2011) 433–446.
- [25] D.B. Miracle, O.N. Senkov, A critical review of high entropy alloys and related concepts, *Acta Mater.* 122 (2017) 448–511.
- [26] C. Kittel (NY). Introduction to Solid State Physics, 8th ed., John Wiley & Sons, New York, 2004.
- [27] A. Takeuchi, A. Inoue, Mixing enthalpy of liquid phase calculated by miedema's scheme and approximated with sub-regular solution model for assessing forming ability of amorphous and glassy alloys, *Intermetallics* 18 (2010) 1779–1789.
- [28] G. Bracq, J.C. Crivello, M.L. Brocq, J.M. Joubert, I. Guillot, What is the enthalpy contribution to the stabilization of the Co-Cr-Fe-Mn-Ni face-centered cubic solid solution, *J. Ph. Equilib. Diffus.* 42 (2021) 561–570.
- [29] Z. Huiting, R. Chen, G. Qin, X. Li, Microstructure evolution, Cu segregation and tensile properties of CoCrFeNiCu high entropy alloy during directional solidification, *J. Mater. Sci. Technol.* 38 (2020) 19–27.
- [30] W.L. Wang, L. Hu, S.B. Luo, L.J. Meng, Liquid phase separation and rapid dendritic growth of high-entropy CoCrCuFeNi alloy, *Intermetallics* 77 (2016) 41–45.
- [31] Y. Tong, K. Jin, H. Bei, J.Y.P. Ko, D.C. Pagan, Y. Zhang, F.X. Zhang, Local lattice distortion in NiCoCr, FeCoNiCr and FeCoNiCrMn concentrated alloys investigated by synchrotron X-ray diffraction, *Mater. Des.* 155 (2018) 1–7.
- [32] Mohamed Arfaoui, György Radnóczki ORCID, Viktória Kovács Kis, Transformations in CrFeCoNiCu High Entropy Alloy Thin Films during In-Situ Annealing in TEM, *Coatings* 10 (1) (2020) 1–15, <https://doi.org/10.3390/coatings10010060>.
- [33] O.N. Senkov, J.M. Scott, S.V. Senkova, D.B. Miracle, C.F. Woodward, Microstructure and room temperature properties of a high-entropy TaNbHfZrTi alloy, *J. Alloy. Compd.* 509 (2011) 6043–6048.
- [34] Y. Jia, L. Zhang, P. Li, X. Ma, L. Xu, S. Wu, Y. Jia, G. Wang, Microstructure and mechanical properties of Nb-Ti-V-Zr refractory medium-entropy alloy, *Front. Mater.* 7 (2020) 172.
- [35] L.A. Gypen, A. Deruyttere, Multi-component solid solution hardening, *J. Mater. Sci.* 12 (1977) 1028–1033.
- [36] G.A. Salishchev, M.A. Tikhonovsky, D.G. Shaysultanov, N.D. Stepanov, A. V. Kuznetsov, I.V. Kolodiy, A.S. Tortika, O.N. Senkov, Effect of Mn and V on structure and mechanical properties of high-entropy alloys based on CoCrFeNi system, *J. Alloy. Compd.* 591 (2014) 11–21.
- [37] T.T. Shun, L.Y. Chang, M.H. Shiu, Microstructures and mechanical properties of multiprincipal component CoCrFeNiTix alloys, *Mater. Sci. Eng. A* 556 (2012) 170–174.
- [38] H. Jiang, L. Jiang, D. Qiao, Y. Lu, Effect of niobium on microstructure and properties of the CoCrFeNbNi high entropy alloys, *J. Mater. Sci. Technol.* 33 (2017) 712–717.
- [39] G. Qin, Z. Li, R. Chen, Z. Huiting, CoCrFeMnNi high-entropy alloys reinforced with Laves phase by adding Nb and Ti elements, *J. Mater. Res.* 34 (2019) 1011–1020.
- [40] N.D. Stepanov, D.G. Shaysultanov, G. Salishchev, M. Tikhonovsky, Effect of V content on microstructure and mechanical properties of the CoCrFeMnNiVx high entropy alloys, *J. Alloy. Compd.* 628 (2015) 170–185.
- [41] G. Qin, R. Chen, Z. Huiting, H. Fang, Strengthening FCC-CoCrFeMnNi high entropy alloys by Mo addition, *J. Mater. Sci. Technol.* 35 (2019) 578–583,33.
- [42] X.F. Wang, Y. Zhang, Y. Qiao, G.L. Chen, Novel microstructure and properties of multicomponent CoCrCuFeNiTix alloys, *Intermetallics* 15 (2007) 357–362.
- [43] G. Qin, S. Wang, R. Chen, X. Gong, Microstructures and mechanical properties of Nb-alloyed CoCrCuFeNi high-entropy alloys, *J. Mater. Sci. Technol.* 34 (2018) 365–369.
- [44] N.D. Stepanov, D.G. Shaysultanov, R. Chernichenko, M. Tikhonovsky, Effect of Al on structure and mechanical properties of Fe-Mn-Cr-Ni-Al non-equiatomic high entropy alloys with high Fe content, *J. Alloy. Compd.* 770 (2019) 194–203.
- [45] Ning Li, Cun-Lei Jia, Zhi-Wei Wang, Li-Hui Wu, Ding-Rui Ni, Zheng-Kun Li, Hua-Meng Fu, Peng Xue, Bo-Lv Xiao, Zong-Yi Ma, Yi Shao, Yun-Long Chang, Achieving a high-strength CoCrFeNiCu high-entropy alloy with an ultrafine-grained structure via friction stir processing, *Acta Metall. Sin.* 33 (2020) 947–956.
- [46] L.A.I. Kestens, H. Pirlgazi, Texture formation in metal alloys with cubic crystal structure, *Mater. Sci. Technol.* 32 (2016) 1303–1315.
- [47] I.A. Bryukhanov, V.A. Emelyanov, Shear stress relaxation through the motion of edge dislocations in Cu and Cu-Ni solid solution: a molecular dynamics and discrete dislocation study, *Comput. Mater. Sci.* 201 (2022), 110885.
- [48] Z.L. Wang, Transmission electron microscopy of shape-controlled nanocrystals and their assemblies, *J. Phys. Chem. B* 104 (2000) 1153–1175.
- [49] F. McKay, Y. Fang, O. Kizilkaya, P. Singh, CoCrFeNi high-entropy alloy as an enhanced hydrogen evolution catalyst in an acidic solution, *J. Phys. Chem. C* 125 (2021) 17008–17018.
- [50] S. Mondal, S. kumar de, R. Jana, A. Roy, M. Mukherjee, A. Datta, B. Satpati, D. Senapati, Unveiling the excellent electrocatalytic activity of grain-boundary enriched anisotropic pure gold nanostructures toward hydrogen evolution reaction: a combined approach of experiment and theory, *ACS Appl. Energy Mater.* 4 (2021) 3017–3032.
- [51] F. Bao, E. Kemppainen, I. Dorbandt, R. Bors, F. Xi, R. Schlattmann, R. van de Krol, S. Calnan, Understanding the hydrogen evolution reaction kinetics of electrodeposited nickel-molybdenum in acidic, near-neutral, and alkaline conditions, *ChemElectroChem* 8 (2021), 195–20.
- [52] Hector Prats, Karen Chan, The determination of the HOR/HER reaction mechanism from experimental kinetic data, *Phys. Chem. Chem. Phys.* 23 (2021) 27150–27158.
- [53] Y. Yang, X. Zhu, B. Zhang, H. Yang, C. Liang, Electrocatalytic properties of porous Ni-Co-WC composite electrode toward hydrogen evolution reaction in acid medium, *Int. J. Hydrot. Energy* 44 (36) (2019) 19771–19781.
- [54] G.S. Frankel, Pitting corrosion of metals: a review of the critical factors, *J. Electrochem. Soc.* 145 (1998) 2186.